

Experimental Observation of a Magnetic Interfacial Effect

Wibson W. G. Silva, Sérgio V. B. Degiorgi and José Holanda*

Programa de Pós-Graduação em Engenharia Física, Universidade Federal Rural de Pernambuco, 54518-430, Cabo de Santo Agostinho, Pernambuco, Brazil.

Abstract

We observed a magnetic interfacial effect due to the coupling between two interfaces of different materials. The interface is composed of an antiferromagnetic and other quasi-ferromagnetic material. This effect we measured through the ferromagnetic resonance technique without and with electric current.

Keywords: Magnetic, non-collinear, uncompensated, interface

Antiferromagnetic materials exhibiting topologically protected states in their momentum-space bands as well as those exhibiting topologically non-trivial real-space at the interface, inspire the production of new devices in antiferromagnetic spintronics [1-6]. A non-collinear antiferromagnet that has a giant magnetocrystalline anisotropy energy of 10 meV per unit cell is the IrMn_3 [7-12]. The IrMn_3 has a giant spin Hall angle (up to ≈ 0.35) in the direction [001] and crystallizes in a face-centered cubic lattice [10]. The local ferromagnetism from uncompensated spins can induce antiferromagnetic symmetry in the adjacent material [4, 13-15]. Platinum (Pt) can be an excellent adjacent material for this coupling because Pt is quasi-ferromagnetic according to Stoner's criterion [16]. Thus, IrMn_3 and Pt are promissory candidates for the detection of resonance signals due to the ferromagnetism at the interface. The detection of these signals can

*Corresponding author: joseholanda.silvajunior@ufrpe.br

be performed using the ferromagnetic resonance (FMR) technique without and with electric current [17-29]. In this Letter, we observe ferromagnetic resonance signals at the sample of IrMn₃/Pt bilayer without and with electric current. Furthermore, we analyzed the change of the interface damping as a function of the electric current.

All IrMn₃ films were epitaxially grown in a magnetron sputtering system with pressures of base approximately 1×10^{-7} torr and of argon of 3 mtorr at a temperature of 843 K on the (100)MgO substrates. We used one Ti(2 nm) layer to protect the surface properties of IrMn₃ or Pt layer. We deposited the Pt layer at 373 K temperature to diffusion on IrMn₃ and the Ti layer at room temperature. **Fig. 1 (a)** shows an X-ray diffraction pattern for IrMn₃ grown on a (100)MgO substrate. We found that IrMn₃ has a lattice constant of (0.377 ± 0.001) nm, which is consistent with previous literature values [30]. The X-ray diffraction pattern of **Fig. 1 (b)** shows that the Pt has grown on the IrMn₃ surface, showing different phases. The quality of samples also were analyzed by transmission electron microscopy (TEM), as shown in the micrograph of the IrMn₃(10 nm)/Pt(6 nm)/Ti(2 nm) sample in **Fig. 1 (c)**.

As it is well known, an exchange bias can be stabilized at room temperature for IrMn₃/Py bilayer, and thus IrMn₃ is antiferromagnetically ordered at room temperature [2, 4, 10]. In the same way, the ferromagnetism in the antiferromagnetic and quasi-ferromagnetic interface is stabilized [28]. For the deposition of samples, we used a metallic mask to avoid any type of contamination on the surface of MgO, and we utilized the laser write technique for the production of the coplanar waveguide on the sample surface, as shown in the **Fig. 1 (d)**. We measured resonance signals by the flip-chip vector network analyzer ferromagnetic resonance (VNA-FMR) technique. We obtained via Lorentz fitting the frequency swept linewidths (Δf_{VNA}). Detailed steps, including the conversion from Δf_{VNA} to the field linewidths ΔH , are shown in ref. [28]. In the process of VNA-FMR, we measured the transmission coefficient by sweeping the frequency at every fixed magnetic field [4].

In the **Fig. 2 (a)**, we show the unit cell of IrMn₃, where the Mn atoms

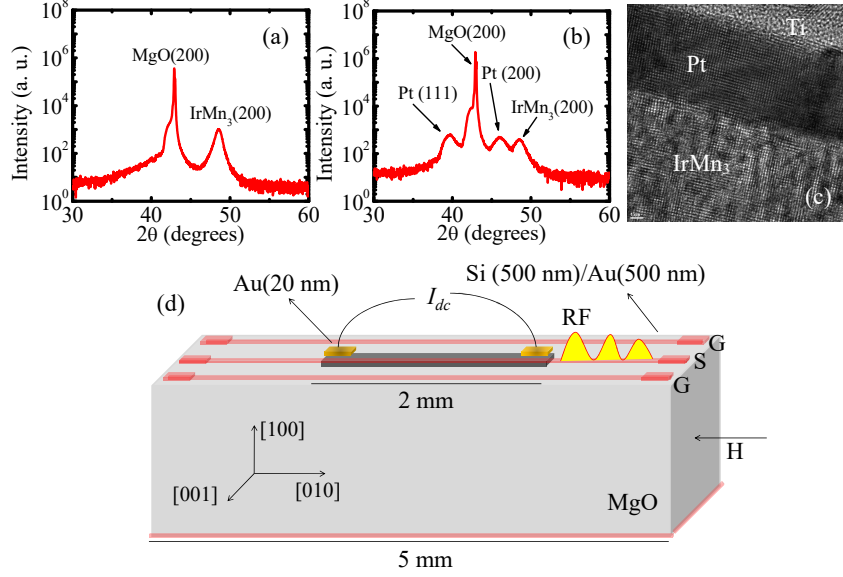


Figure 1: (Color online) X-ray diffraction pattern measured for a 10 nm thick IrMn₃ layer without or with a 6 nm thick Pt layer capped with a 2-nm Ti layer: **(a)** IrMn₃(10 nm)/Ti(2 nm) and **(b)** IrMn₃(10 nm)/Pt(6 nm)/Ti(2 nm). **(c)** Transmission Electron Microscopy (TEM) micrograph of IrMn₃(10 nm)/Pt(6 nm)/Ti(2 nm). **(d)** Shows the coplanar waveguide (CPW) deposited by Electron Beam Evaporation at the up of the samples for measures of ferromagnetic resonance without and with electric current.

are on the $\{111\}$ planes and their spins are aligned along the $\langle 112 \rangle$ directions. As it is known, spins-in and spins-out configurations are nonequivalent ground states and are chiral images of each other [3, 4, 23]. For analyses of the spins-in or spins-out configurations, a transversal section can be made in the unit cell of IrMn₃ shown from a kagome lattice in the (111) plane with either pointing outwards in each triangular Mn arrangement (see the **Fig. 2 (b)**). This configuration represents the interface configuration of the spins-out for the film. In this case, the thin layer of Pt deposited on top of the IrMn₃ grows with [100] and [111] crystallographic directions (see the **Fig. 1 (b)**).

The net chirality at the IrMn₃/Pt interface in the resonance condition can be

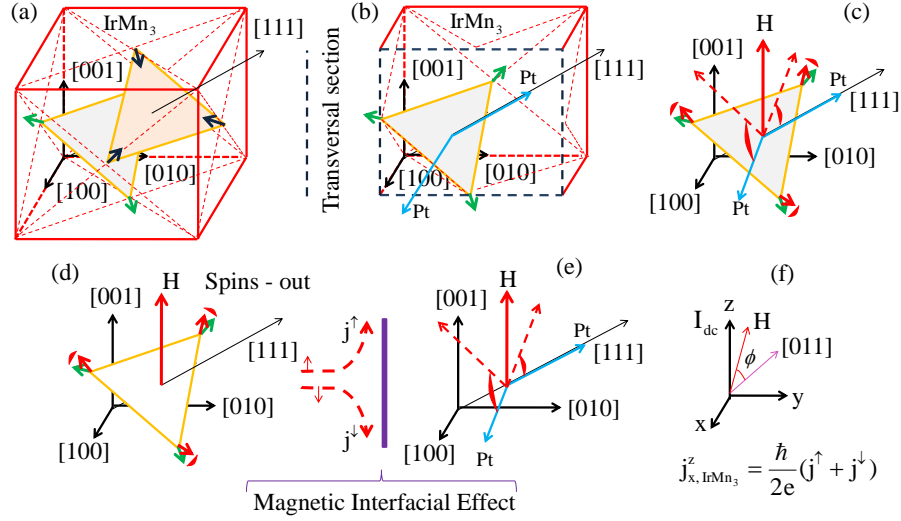


Figure 2: (Color online)(a) Show the unit cell of IrMn₃ whose moments Mn are parallel to the planes {111} and aligned with the directions $\langle 112 \rangle$. (b) The transversal section in which the interface configuration of the spins-out for IrMn₃. (c) Configuration of resonance condition of the rotation of spins of IrMn₃ and Pt on a magnetic field. (d) Arrangement from the magnetic interfacial effect of IrMn₃ in interface resonance condition, where a spin accumulation is created in the direction from Pt. (e) Arrangement from spin Hall effect of Pt in interface resonance condition, where a spin accumulation is created in the direction from IrMn₃. (f) Coordinates system of the spin currents of the antiferromagnet IrMn₃.

understood by the rotation of uncompensated spins of IrMn₃, and the spins at the surface of Pt, as shown in **Fig. 2 (c)**. The coupling of the noncollinear spins of IrMn₃, and the quasi-ferromagnetic spins of the Pt represent the ideal condition to explore the magnetic interface. [3, 4, 23, 29-35]. In resonance condition using the Hall effects of the IrMn₃ (see **Fig. 2 (d)**) and of the Pt (see **Fig. 2 (e)**), a spin accumulation field is created as two spin currents flowing at directions of the interface [4, 23]. The polarization of the spin accumulation

field defined by the magnetic field is transversal at the magnetic interface, as shown in **Figs. 2 (d) and (e)**. The spin current of the IrMn₃ is defined as $j_{IrMn_3}^z = j_{y,SSS}^z = (j^\uparrow + j^\downarrow)\hbar/2e$, which depend of the spins-in and spins-out configurations, as shows the **Fig. 2 (f)**.

The efficiency from the FMR signals is due to the net chirality of the spin structures, which provides more complexity compared to non-magnetic materials [29-36]. **Fig. 3 (a)** shows the FMR signals obtained with a VNA for one frequency of 10 GHz, magnetic field of 10.3 kOe, and different electric currents -1, 0, and +1 mA. Two observations need highlight: first, the electric current produces a significant variation in frequency swept linewidths (Δf_{VNA}), and second, a shift is caused by the accumulation field (H_{Ac}). In **Fig. 3 (b)** we show that the accumulation field (H_{Ac}) due to the electric current produces a modification in the resonance field. This is clear evidence of a magnetic interfacial effect due to the strong coupling at interface IrMn₃/Pt interface, similar to the IrMn₃/Py bilayer [4, 12, 19]. The solid curve represents the fit from the experimental data to the Kittel equation, $f = \gamma[(H_R)(H_R + 4\pi M_{eff} \pm H_{Ac})]^{1/2}$, where the gyromagnetic ratio is $(\gamma_{IrMn_3/Pt})/\gamma_{IrMn_3/Py} = 5\%$, the spectroscopic splitting factor calculated considering the Stoner's criterion [16] is $g_{IrMn_3/Pt}/g_{IrMn_3/Py} = 5\%$, μ_B is the Bohr magneton, \hbar is the reduced Planck constant, and $4\pi M_{eff} = 4\pi M_S + H_{AS}$ is the effective magnetization that is much larger than the saturation magnetization $4\pi M_S$ due to the effect of the surface anisotropy field H_{AS} . Using the fit with the Kittel equation to zero electric currents, we obtained for effective magnetization $4\pi M_{eff} = (523.78 \pm 0.005)$ kOe, which is smaller than that obtained for *IrMn₃/Py* bilayer [4, 10, 12, 19].

The properties of noncollinear antiferromagnetic materials with magnetic topological states yield large changes [31-35], this also is a characteristic of uncompensated spins that induces magnetism. In the **Fig. 4 (a)**, we represent the change from resonance frequency as a function of the spin accumulation field (H_{Ac}) for electric current ± 1 mA. The spin accumulation field increase by obeying a Kittel equation describes by greens lines. In this case, the spins-in and spins-out configurations exhibit the same energies, and both exist spontaneously

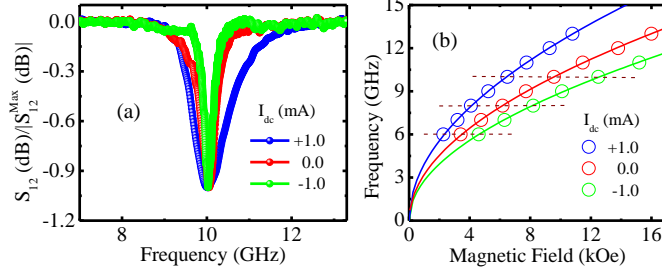


Figure 3: (Color online) **(a)** Ferromagnetic resonance (FMR) signals were obtained using a VNA for one frequency of 10 GHz, magnetic field of 10.3 kOe, and different electric currents -1, 0, and +1 mA. **(b)** FMR frequency as a function of the magnetic field, which the accumulation field (H_{Ac}) due to the electric current produces a change in the resonance field. The fits are performed with the Kittel equation, where $(\gamma_{IrMn_3/Pt})/\gamma_{IrMn_3/Pt} = 5\%$ and $4\pi M_{eff} = (523.78 \pm 0.005)$ kOe.

in the material [31]. On the other hand, in the **Fig. 4 (b)** we show the spin accumulation field as a function of electric current in the resonance frequency of 10 GHz. A small onset of saturation of the spin accumulation field is observed for electric currents $I_{dc} < -1$ mA and $I_{dc} > +1$ mA, which is also observed in other bilayers [4, 10, 11, 27]. The polarization from the spin accumulation field obeys the electric current confirming the process from the manipulation of the magnetic interfacial effect in the IrMn₃/Pt bilayer, similar to the manipulation of the exchange bias at the antiferromagnetic/ferromagnetic bilayer [4, 12, 19]. In the **Fig. 4 (c)**, the fit is made with the expression $\Delta H = (\alpha/\gamma)f$ [33], where α is the magnetic Gilbert damping of the interface.

In the **Fig. 4 (d)**, we show the change of the damping of the IrMn₃/Pt bilayer as a function of the electric current. Damping starts to increase for electric currents below -1 mA, as well as decreases for electric currents above +1 mA. This behavior agrees with the data of the **Fig. 4 (b)**, and is due to the spins-in and spins-out configurations in the IrMn₃/Pt bilayer that loses their dynamic characteristics due to the saturation of the spin accumulation field and the fact that the interface presents a local temperature change [12,

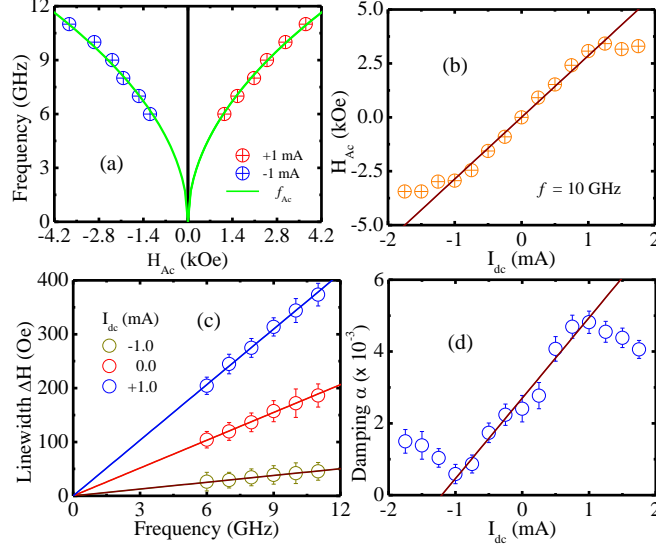


Figure 4: (Color online) **(a)** Ferromagnetic resonance (FMR) frequency as a function of the spin accumulation field H_{Ac} . The fits are performed with the Kittel equation. **(b)** Spin accumulation field as a function of the electric current to the frequency of 10 GHz. **(c)** Shows the linewidth change as a function of the FMR frequency to three values of electric current -1, 0, +1 mA. **(d)** Damping change as a function of electric current.

19]. In summary, we experimentally observed a magnetic interfacial effect in IrMn₃/Pt bilayer, and we manipulated it through the FMR technique without and with electric current.

Acknowledgements

This research was supported by Conselho Nacional de Desenvolvimento Científico e Tecnológico (CNPq), Coordenação de Aperfeiçoamento de Pessoal de Nível Superior (CAPES), Financiadora de Estudos e Projetos (FINEP), and Fundação de Amparo à Ciência e Tecnologia do Estado de Pernambuco (FACEPE).

References

- [1] J. Zelezny, Y. Zhang, C. Felser, and B. Yan. Spin-polarized current in noncollinear antiferromagnets. *Phys. Rev. Lett.* **119**, 187204 (2017).
- [2] S. Jenkins, R. W. Chantrell, T. J. Klemmer, and R. F. L. Evans. Magnetic anisotropy of the noncollinear antiferromagnet IrMn₃. *Phys. Rev.* **B 100**, 220405(R) (2019).
- [3] V. T. N. Huyen, M.-T. Suzuki, K. Yamauchi, and T. Oguchi. Topology analysis for anomalous Hall effect in the noncollinear antiferromagnetic states of Mn₃AN (A = Ni, Cu, Zn, Ga, Ge, Pd, In, Sn, Ir, Pt). *Phys. Rev.* **B 100**, 094426 (2019).
- [4] J. Holanda, H. Saglam, V. Karakas, Z. Zhang, Y. Li, R. Divan, Y. Liu, O. Ozatay, V. Novosad, J. E. Pearson, A. Hoffmann. Magnetic damping modulation in IrMn₃/Ni₈₀Fe₂₀ via the magnetic spin Hall effect. *Phys. Rev. Lett.* **124**, 087204 (2020).
- [5] M. Kimata, H. Chen, K. Kondou, S. Sugimoto, P. K. Muduli, M. Ikhlas, Y. Omori, T. Tomita, A. H. MacDonald, S. Nakatsuji and Y. Otani. Magnetic and magnetic inverse spin Hall effects in a non-collinear antiferromagnet. *Nature* **565**, 627 (2019).
- [6] Y. Deng, X. Liu, Y. Chen, Z. Du, N. Jiang, C. Shen, E. Zhang, H. Zheng, H.-Z. Lu, K.u Wang, All-electrical switching of a topological non-collinear antiferromagnet at room temperature, *National Science Review*, nwac154, <https://doi.org/10.1093/nsr/nwac154> (2022).
- [7] J. Zelezný, P. Olejník, A. Hoffmann and H. Ohno. Spin transport and spin torque in antiferromagnetic devices. *Nature Phys.* **14**, 220 (2018).
- [8] A. Neubauer, C. Pfleiderer, B. Binz, A. Rosch, R. Ritz, P. G. Niklowitz, and P. Böni. Topological Hall effect in the A phase of MnSi. *Phys. Rev. Lett.* **102**, 186602 (2009) and *Phys. Rev. Lett.* **110**, 209902 (2013).

- [9] S. Nakatsuji, N. Kiyohara, T. Higo. Large anomalous Hall effect in a non-collinear antiferromagnet at room temperature. *Nature* **527**, 212 (2015).
- [10] W. Zang, W. Han, S.-H. Yang, Y. Sun, Y. Zhang, B. Yan, S. S. P. Parkin. Giant facet-dependent spin-orbit torque and spin Hall conductivity in the triangular antiferromagnet IrMn₃. *Sci. Adv.* **2**, e1600759 (2016).
- [11] H. Tsai, T. Higo, K. Kondou, T. Nomoto, A. Sakai, A. Kobayashi, T. Nakano, K. Yakushiji, R. Arita, S. Miwa, Y. Otani and S. Nakatsuji, Electrical manipulation of a topological antiferromagnetic state, *Nature* **580**, 608 (2020).
- [12] J. Holanda, D. S. Maior, A. Azevedo, S. M. Rezende. Anisotropic magnetoresistance and anomalous Nernst effect in exchange biased permalloy/(100)NiO single-crystal. *Jour. Magn. Magn. Mater.* **432**, 507 (2017).
- [13] L. Liu, Y. Li, Y. Liu, T. Feng, J. Xu, X. R. Wang, D. Wu, P. Gao, and J. Li, Interfacial modulation of spin pumping in YIG/Pt, *Phys. Rev.* **B 102**, 014411 (2020).
- [14] N. Mohanta, S. Okamoto and E. Dagotto, Skyrmion control of Majorana states in planar Josephson junctions, *Commun Phys* **4**, 163 (2021).
- [15] Z. Zhang, M. Vogel, J. Holanda, M. B. Jungfleisch, C. Liu, Y. Li, J. E. Pearson, R. Divan, W. Zhang, A. Hoffmann, Y. Nie, and V. Novosad, Spin-wave frequency division multiplexing in an yttrium iron garnet microstripe magnetized by inhomogeneous field, *Appl. Phys. Lett.* **115**, 232402 (2019).
- [16] L. Liang, Q. Chen, J. Lu, W. Talsma, J. Shan, G. R. Blake, T. T. M. Palstra, J. Ye. Inducing ferromagnetism and Kondo effect in platinum by paramagnetic ionic gating. *Sci. Adv.* **4**, eaar2030 (2018).
- [17] P. Wadley, B. Howells, J. Železný, C. Andrews, V. Hills, R. P. Campion, V. Novák, K. Olejník, F. Maccherozzi, S. S. Dhesi, S. Y. Martin, T. Wagner, J. Wunderlich, F. Freimuth, Y. Mokrousov, J. Kuneš, J. S. Chauhan, M.

- J. Grzybowski, A. W. Rushforth, K. W. Edmonds, B. L. Gallagherand, T. Jungwirth. Electrical switching of an antiferromagnet. *Science* **351**, 587 (2016).
- [18] J. E. Hirsch. Spin Hall Effect. *Phys. Rev. Lett.* **83**, 1834 (1999).
- [19] W. Zhang, W. Han, Xin Jiang, S.-H. Yang and S. S. P. Parkin. Role of transparency of platinum-ferromagnet interfaces in determining the intrinsic magnitude of the spin Hall effect. *Nature Phys.* **11**, 496 (2015).
- [20] Y. Li, N. Kanazawa, X. Z. Yu, A. Tsukazaki, M. Kawasaki, M. Ichikawa, X. F. Jin, F. Kagawa, and Y. Tokura. Robust formation of skyrmions and topological Hall effect anomaly in epitaxial thin films of MnSi. *Phys. Rev. Lett.* **110**, 117202 (2013).
- [21] Y. Taguchi, Y. Oohara, H. Yoshizawa, N. Nagaosa, Y. Tokura. Spin chirality, Berry phase, and anomalous Hall effect in a frustrated ferromagnet. *Science* **291**, 2573–2576 (2001).
- [22] Y. Machida, S. Nakatsuji, S. Onoda, T. Tayama, T. Sakakibara. Time-reversal symmetry breaking and spontaneous hall effect without magnetic dipole order. *Nature* **463**, 210–213 (2010).
- [23] J. B. S. Mendes, R. O. Cunha, O. Alves Santos, P. R. T. Ribeiro, F. L. A. Machado, R. L. Rodríguez-Suárez, A. Azevedo, and S. M. Rezende. Large inverse spin Hall effect in the antiferromagnetic metal Ir₂₀Mn₈₀. *Phys. Rev. B* **89**, 140406(R) (2014).
- [24] A. Hoffmann. Spin Hall Effects in Metals. *IEEE Trans. Magn.* **49**, 5172 (2013).
- [25] L. Liu, C.-F. Pai, Y. Li, H. W. Tseng, D. C. Ralph, and R. A. Buhrman. Spin-torque switching with the giant spin Hall effect of tantalum. *Science* **336**, 555 (2012).

- [26] T. Higo, D. Qu, Y. Li, C. L. Chien, Y. Otani, and S. Nakatsuji. Anomalous Hall effect in thin films of the Weyl antiferromagnet Mn_3Sn . *Appl. Phys. Lett.* **113**, 202402 (2018).
- [27] A. Kohn, A. Kovács, R. Fan, G. J. McIntyre, R. C. C. Ward and J. P. Goff. The antiferromagnetic structures of IrMn_3 and their influence on exchange-bias. *Scientific Reports* **3**, 7 (2013).
- [28] J. Holanda, O. Alves Santos, R. L. Rodríguez-Suárez, A. Azevedo, S. M. Rezende, Simultaneous spin pumping and spin Seebeck experiments with thermal control of the magnetic damping in bilayers of yttrium iron garnet and heavy metals: YIG/Pt and YIG/IrMn , *Physical Review B* **95**, 134432 (2017).
- [29] L. Smejkal, Y. Mokrousov, B. Yan and A. H. MacDonald. Topological antiferromagnetic spintronics. *Nature Phys.* **14**, 242 (2018).
- [30] W. Jiang, P. Upadhyaya, W. Zhang, G. Yu, M. B. Jungfleisch, F. Y. Fradin, J. E. Pearson, Y. Tserkovnyak, K. L. Wang, O. Heinonen, S. G. E. te Velthuis, A. Hoffmann. Blowing magnetic skyrmion bubbles. *Science*. **6245**, 283 (2015).
- [31] Y. Liu, Y. Liu, M. Chen, S. Srivastava, P. He, K. L. Teo, T. Phung, S.-H. Yang, and H. Yang. Current-induced out-of-plane spin accumulation on the (001) surface of the IrMn_3 antiferromagnet. *Phys. Rev. Appl.* **12**, 064046 (2019).
- [32] M. Mogi. A magnetic heterostructure of topological insulators as a candidate for an axion insulator. *Nat. Mater.* **16**, 516 (2017).
- [33] Y. Tokura, M. Kawasaki, N. Nagaosa. Emergent functions of quantum materials. *Nat. Phys.* **13**, 10561068 (2017).
- [34] H. Chen, Q. Niu, and A. H. MacDonald. Anomalous Hall effect arising from noncollinear antiferromagnetism. *Phys. Rev. Lett.* **112**, 017205 (2014).

- [35] C. Surgers, G. Fischer, P. Winkel and H. V. Lohneysen. Large topological Hall effect in the noncollinear phase of an antiferromagnet. *Nat. Commun.* **5**, 3400 (2014).
- [36] T. L. Gilbert. A phenomenological theory of damping in ferromagnetic materials. *IEEE Trans. Magn.* **40**, 3443 (2004).